molecules

MDPI

Review

MoS_2 as a Co-Catalyst for Photocatalytic Hydrogen Production: A Mini Review

Sayyar Ali Shah, Iltaf Khan * and Aihua Yuan *

School of Environmental & Chemical Engineering, Jiangsu University of Science and Technology, Zhenjiang 212100, China; sayyar786@gmail.com
* Correspondence: 202200000032@just.edu.cn (I.K.); aihua.yuan@just.edu.cn (A.Y.)

Abstract: Molybdenum disulfide (MoS_2), with a two-dimensional (2D) structure, has attracted huge research interest due to its unique electrical, optical, and physicochemical properties. MoS_2 has been used as a co-catalyst for the synthesis of novel heterojunction composites with enhanced photocatalytic hydrogen production under solar light irradiation. In this review, we briefly highlight the atomic-scale structure of MoS_2 nanosheets. The top-down and bottom-up synthetic methods of MoS_2 nanosheets are described. Additionally, we discuss the formation of MoS_2 heterostructures with titanium dioxide (TiO_2), graphitic carbon nitride (g-C_3N_4), and other semiconductors and co-catalysts for enhanced photocatalytic hydrogen generation. This review addresses the challenges and future perspectives for enhancing solar hydrogen production performance in heterojunction materials using MoS_2 as a co-catalyst.

Keywords: photocatalysis; heterojunction; layers structure materials; hydrogen production

Citation: Shah, S.A.; Khan, I.; Yuan, A. MoS_2 as a Co-Catalyst for Photocatalytic Hydrogen Production: A Mini Review. *Molecules* **2022**, *27*, 3289. https://doi.org/10.3390/molecules27103289

Academic Editor: Muhammad Humayun

Received: 4 April 2022
Accepted: 17 May 2022
Published: 20 May 2022

1. Introduction

Hydrogen is a clean, renewable energy source and alternative to fossil fuels [1] that can be stored at high mass-specific energy density, and its only product on combustion is water [2]. At present, about 96% of hydrogen is industrially produced from coal gasification and steam methane reformation processes [1,2]. However, these processes of hydrogen production also generate secondary pollutants or greenhouse gases, such as CO_2 and N_2O, that affect the environment [2]. Methane pyrolysis produces hydrogen and solid carbon as a byproduct [3]. This process generates CO_2-free hydrogen and has an advantage over conventional steam methane reformation and coal gasification processes. However, methane pyrolysis is a temporary solution and not a sustainable process due to the depletion of natural gas reserves [3].

To overcome energy challenges and environmental problems, hydrogen production from electrochemical water splitting using highly active catalysts is a promising strategy [4,5]. Less than 4% of hydrogen is produced through electrocatalysis at the industrial level [2]. The electrocatalysis of water for hydrogen production is a high-cost technique, which has hindered its large-scale industrialization. As an alternative, photocatalytic hydrogen evolution reaction (HER) from water splitting over a particular semiconductor material has been the most interesting way to address these issues. Generally, the photocatalytic efficiency depends upon three processes, including light absorption in the solar spectrum, charge separation, and surface active sites for catalytic activity [1,2,6].

A photocatalyst that can absorb sunlight across the whole solar spectrum is considered to be an ideal candidate for photocatalysis [6,7]. In 1972, Fujishima et al. reported photo-induced water splitting on TiO_2 electrodes [8]. Since then, much research has been focused on TiO_2 and other related semiconducting materials such as metal oxides, metal sulfides, conjugated polymers, nanosheets, graphitic carbon nitride, metal organic frameworks, and covalent organic frameworks, etc., as photocatalysts for hydrogen production [9–17].

However, the available photocatalysts for hydrogen production are still limited due to low visible light absorption and high electron–hole recombination rates.

Molybdenum disulfide (MoS_2), with a 2D nanostructure, has attracted huge attention due to its outstanding optical and electronic properties and promising applications [18–22]. MoS_2 nanomaterials as co-catalysts are promising photocatalysts for HER [18,23]. It is reported that the exposed edges of layers of MoS_2 contain active sites for catalytic activity while its basal planes are mostly inactive [19,24]. In addition to the active photocatalytic sites, the band gap of MoS_2 nanosheets is an important parameter for photocatalytic HER. The band gap of MoS_2 increases from bulk (1.2 eV) to single layer (1.9 eV) due to quantum confinement [19,24]. As a result, the location of the conduction band (CB) of MoS_2 moves towards a more negative potential than the proton reduction potential (H^+/H_2), which consequently enhances the reduction in adsorbed H^+ and photocatalytic hydrogen evolution.

It is widely reported that loading a co-catalyst over semiconductors is a promising approach with superior photocatalytic performance due to the photoelectron separation and charge transfer [18,19]. MoS_2-decorated semiconductor materials constitute a promising approach that has shown superior hydrogen production due to their heterojunctions with controllable nanoscale architectures, design for enhanced performance in terms of light absorption, charge separation, and surface catalytic reactions [15,19,23,24].

In this review, we briefly introduce the basic aspects and synthetic methods of MoS_2 nanosheets. Different types of MoS_2-based heterojunction composites are also discussed. The role of MoS_2 nanomaterials as co-catalysts in heterojunction composites for enhanced HER performance is addressed. Additionally, some important issues are highlighted and useful opinions are discussed to further improve photocatalytic hydrogen production using MoS_2 as a co-catalyst.

2. Atomic-Scale Structure of MoS_2

A single layer of MoS_2 has a sandwich structure of S-Mo-S, where the Mo atoms are covalently bonded with the S atoms (Figure 1). MoS_2 has several polymorphs, including $1T_1$, $1T_2$, 1H, 2T, 2H, $2R_1$, $2R_2$, $3H_a$, $3H_b$, 3R, and 4T [25–29]. Among them the 1T MoS_2, 2H MoS_2, and 3R-MoS_2 polymorphs of MoS_2 have been most investigated for different applications [25,27–29]. A single-layer 1T MoS_2 sheet is metallic and has good electrical properties [30,31], while single-layer 2H MoS_2 and 3R-MoS_2 sheets behave as a semiconductor with a direct band gap [28,32].

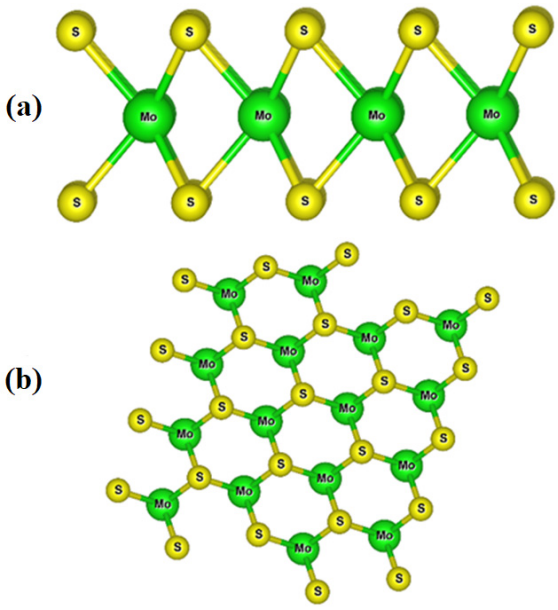

Figure 1. (**a**) Side and (**b**) top views of MoS_2 single layer.

Generally, MoS_2 sheets are stacked together by weak van der Waals forces and form few-layer MoS_2 nanosheets. As the band gap of MoS_2 nanosheets increases from bulk (1.2 eV) to single layer (1.9 eV) [33], it absorbs the visible region of the solar spectrum. Thus, MoS_2 can play an important role as a co-catalyst during photocatalysis [29]. MoS_2-based semiconductor composites act as co-catalysts that can significantly enhance the efficiency of photocatalytic hydrogen production [7,34–37].

3. Photochemical Hydrogen Evolution Reaction

As mentioned above, Fujishima and Honda reported on photo-induced water splitting on TiO_2 electrodes. Hydrogen can also be directly produced from photochemical water splitting. Usually, a photoelectrolytic cell is designed to carry out the photochemical water splitting process. A typical photoelectrolytic cell for water splitting is shown in Figure 2a [38]. Using light sources, the photocatalytic water splitting takes place in several steps: the absorption of light by catalyst on electrode; the generation of charges followed by the excitation of electrons in the valence band; the separation of charge as well as the transport of charge carriers; and the oxidation of water and generation of hydrogen during water splitting, which occur at separate electrodes. The pure, overall water splitting process comprises two half-reactions to generate hydrogen and oxygen molecules, as shown in Figure 2b [39]. Water oxidation occurs at the anode to produce oxygen, whereas H^+ ions are reduced on the cathode into hydrogen gas. For more details of photocatalytic water splitting, see the review of Jeong et al. [39].

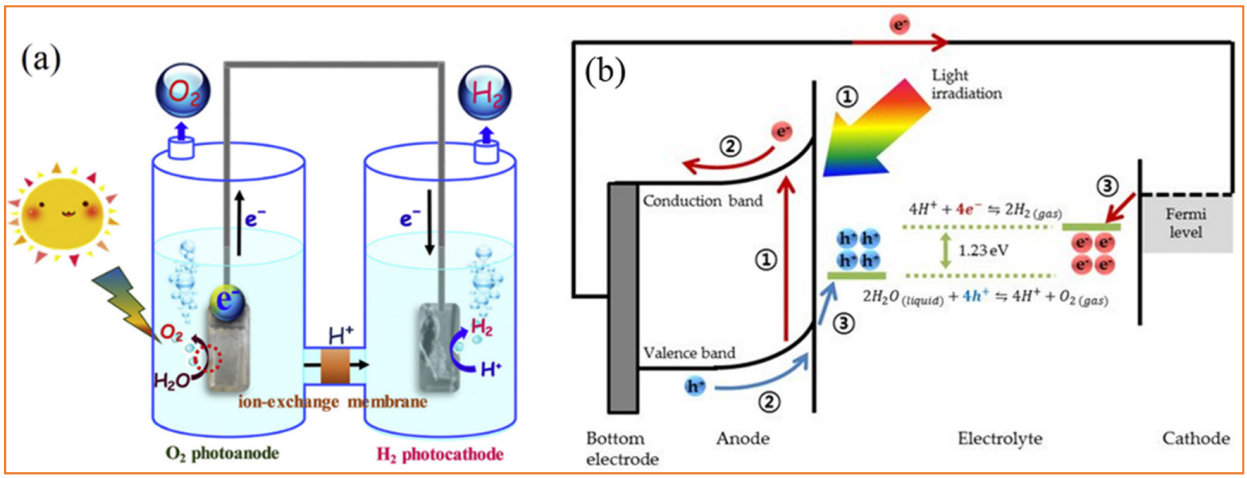

Figure 2. (**a**) Schematic device illustration of photoelectrochemical water splitting. Reprinted with permission from Ref. [38] (Copyright 2019 Elsevier). (**b**) Schematic representation of the photoelectrochemical water splitting process in a common PEC water splitting system consisting of a photoanode and a metal counterpart. Reprinted from Ref. [39].

4. Synthesis of MoS_2

Nanostructured MoS_2 can be fabricated via both top-down and bottom-up approaches. In the case of the top-down method, the commercially available bulk crystal of MoS_2 is physically downsized into MoS_2 nanomaterials (Figure 3) [29,40,41], while in the bottom-up approach, MoS_2 nanomaterials are synthesized via chemical reaction with small molecules using chemical vapor deposition (CVD) and hydrothermal or solvothermal methods, etc. [42–44]. Single layers, multilayers, nanoparticles, and quantum dots of MoS_2 have also been reported [45–48]. Continued efforts have been reported for the fabrication of MoS_2 nanomaterials via the top-down and bottom-up strategies [16–19,28–31,40–44].

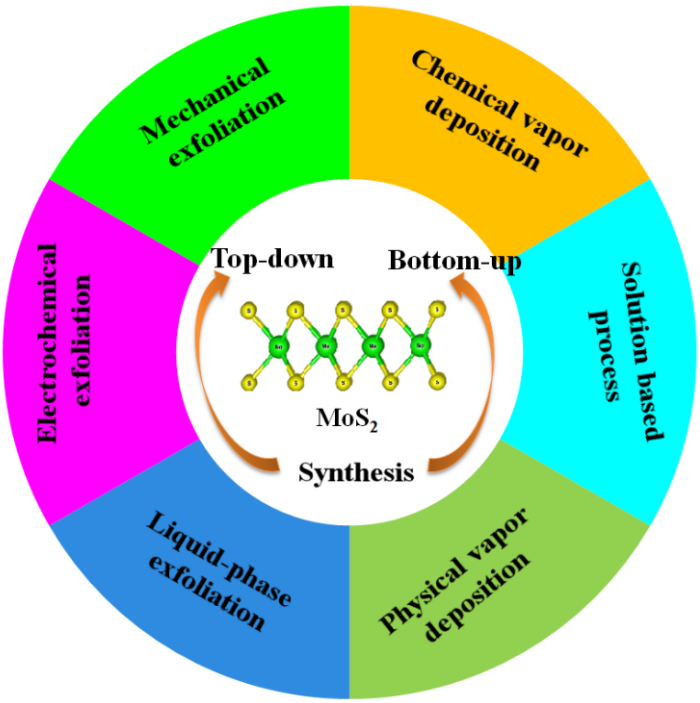

Figure 3. Various synthetic methods for MoS_2 preparation.

4.1. Top-Down Approach

Exfoliation of MoS_2

Due to the layered structure and van der Waals interactions, MoS_2 nanosheets can be easily prepared through the exfoliation method. Mechanical, chemical, electrochemical, and liquid-phase exfoliation processes have been reported for the synthesis of MoS_2 nanosheets [39–52]. For example, in the mechanical exfoliation technique, the suitable MoS_2 flakes are peeled off from the bulk crystal of MoS_2 using adhesive tape and shifted onto a specific substrate [46,53]. When the scotch tape is detached, some parts of MoS_2 remain on the substrate. As result, single- or few-layer MoS_2 nanosheets with random shapes and sizes are obtained. The 2D materials prepared by the exfoliation method have good quality and allow to study the pristine properties of materials and device performance. However, during this process, the thickness and size of the MoS_2 are difficult to control, and the resulting materials are inappropriate for large-scale production and scaled-up applications [53,54]. Li et al., mechanically exfoliated single- and multilayer MoS_2 nanosheets from SiO_2/Si with the adhesive tape method [41]. The flakes of MoS_2 were mechanically stripped on Si/SiO_2 substrate. The obtained single-layer and multilayer MoS_2 materials were characterized using a bright-field optical microscope and an atomic force microscope (AFM). From the AFM measurements, the height of a single MoS_2 sheet was found to be 0.8 nm, while the thickness of two, three, and four layers of MoS_2 nanosheets was 1.5, 2.1, and 2.9 nm, respectively (Figure 4). The MoS_2 nanosheet monolayers showed an enhanced optical performance, especially single-layer MoS_2 nanosheets. It was observed that the van der Waals interactions between MoS_2 to SiO_2 were much weaker. For this purpose, gold can be used as a substrate to exfoliate the MoS_2 nanosheets due to its strong affinity for sulfur. It can exfoliate the MoS_2 monolayer from the bulk because of the strong van der Waals interactions between Au and MoS_2 layers [55–57]. Huang et al. prepared large-area MoS_2 nanosheets using a Au-assisted exfoliation strategy [50]. In a typical synthesis, a Au thin layer was deposited on a Ti or Cr adhesion-covered substrate. To develop good contact between a MoS_2 bulk crystal on tape and a Au-covered substrate, it should be passed under high pressure. The monolayer sheets with a large area were collected from the surface of the Au after peeling off the tape.

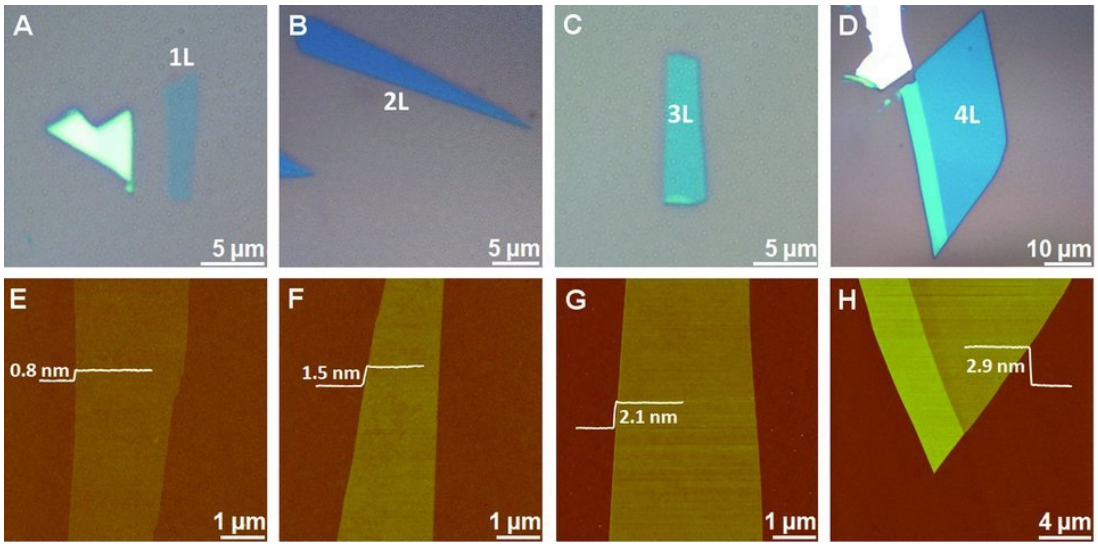

Figure 4. Mechanically exfoliated single- and multilayer MoS_2 nanosheets on Si/SiO_2. (**A**–**D**) Optical microscope and (**E**–**H**) AFM images of MoS_2 nanosheets. The single MoS_2 sheet thickness is 0.8 nm (**E**), while the thickness of two (**F**), three (**G**), and four (**H**) layers of MoS_2 nanosheets is 1.5, 2.1, and 2.9 nm, respectively. Reprinted with permission from Ref. [41]. Copyright 2012 Wiley-VCH Verlag GmbH & Co.

In the top-down approaches, single- and multilayer MoS_2 nanosheets are prepared, which have been used to study some fundamental properties of MoS_2 nanosheets.

4.2. Bottom-Down Approach

4.2.1. Chemical Vapor Deposition

The CVD technique has a long history and is commonly used for the synthesis of high-quality semiconductor materials. In a typical CVD process of MoS_2 nanosheets, the Mo sources are solid precursors of Mo or MoO_3 powder, and the S sources are H_2S gas or solid S powder [58–61]. The solid MoO_3 and vaporized S react with each other in a low-pressure chamber, forming nuclei for the growth of MoS_2 [58]. Then, MoS_2 slowly grows and enlarges its size on the substrates under carrier gas flow. The temperatures at which MoS_2 grows during the CVD process are usually between 700 and 1000 °C, with a metal catalyst such as Au [61]. Plasma-enhanced CVD requires a low temperature (150–300 °C) for the growth of MoS_2 nanosheets, and MoS_2 can even be directly deposited on the plastic substrate [62]. Recently, metal organic CVD has been reported for the synthesis of MoS_2 nanosheets [63,64], where organometallic precursors were used as starting materials.

4.2.2. Physical Vapor Deposition

Advanced technology such as molecular beam epitaxy (MBE) can be used to prepare single-crystal semiconductor thin films. However, its applications are limited to the synthesis of 2D materials [65]. Ordinary physical vapor deposition is rarely reported for 2D materials. A MoS_2–Ti composite was prepared by direct current magnetron sputtering, using Ti and MoS_2 materials [66]. In this process, the MoS_2 was amorphous.

4.2.3. Solution-Based Process

Solution-based processes are commonly used to synthesize MoS_2 nanosheets. Hydrothermal and solvothermal methods are the most interesting for the preparation of MoS_2 nanosheets [67,68]. In these methods, the Mo source is commonly a molybdate, such as Na_2MoO_4 or $(NH_4)_6Mo_7O_{24}$, and the S source is thiourea and thioacetamide and L-cysteine [69–73]. The molybdate reacts with the S or S compound in a stainless steel autoclave. The physicochemical reaction takes place at high temperatures (160–200 °C) and

pressure for at least a few hours. In the solvothermal method, organic solvents such as 1-methyl-2-pyrrolidinone, N,N-dimethylformamide, and polyethylene glycol-600 are used to proceed with the reaction, while in the hydrothermal method, water is used as a solvent. The MoS_2 powders obtained from these methods have different sizes and shapes. The sizes and shapes of the products can be adjusted by altering the experimental conditions. To improve the crystalline quality of MoS_2, the products are usually post-annealed at high temperature.

The MoS_2 nanomaterials prepared through different bottom-up approaches have various sizes, shapes, morphologies, and thicknesses and can be used for many applications.

5. Application of MoS_2 as a Co-Catalyst in Photocatalysis for Hydrogen Production

5.1. MoS_2/Titanium Dioxide Composites

The semiconducting material titanium dioxide (TiO_2) has been employed for hydrogen production due to its good UV light response, non-toxic nature, low cost, chemical stability, and good availability [1,12,24]. However, the photocatalytic energy conversion efficiency of TiO_2 for hydrogen production is low due to its wide band gap structure (Eg $\approx$ 3.2 eV), photogenerated charge recombination, and some reverse reactions [1,2,12,24]. Many strategies have been attempted to improve the catalytic activity of TiO_2 nanomaterials, including micro/nanostructure constructing, crystal facet, crystal phase, surface, and tailoring the band gap [9,74,75], but the photocatalytic activity of TiO_2 still cannot reach the expected efficiency.

MoS_2 is considered a potential co-catalyst for TiO_2 materials to boost the efficiency of photocatalytic hydrogen production. Zhu and his coworkers fabricated MoS_2/TiO_2 photocatalysts with various compositions through a facial mechanochemistry method [76]. The photocatalytic activity of the prepared composite was studied for hydrogen generation under UV irradiation. The 4% MoS_2 loaded on TiO_2 (4%-MoS_2/TiO_2) showed maximum hydrogen production at a rate of 150.7 μmol h^{-1}, which is about 48.6 times higher than that of pure TiO_2 at ~3.1 μmol·h^{-1}. The improved photocatalytic activity of MoS_2/TiO_2 composites is mainly due to electron transfer from TiO_2 to MoS_2 nanosheets and the active sites that produce hydrogen. Meanwhile, the recombination rate of electron–hole pairs is also reduced. Furthermore, the relatively good conductivity of MoS_2 nanosheets also assisted the photo-induced charge separation, leading to an enhanced photocatalytic performance. Ma et al. reported flower-like MoS_2/TiO_2 nanohybrid composite photocatalysts obtained from a metal organic framework-derived precursor via facial hydrothermal methods [77]. The flower-like morphology of the MoS_2/TiO_2 composites was confirmed from SEM images, as shown in Figure 5. In order to investigate the photocatalytic activity, the experiments were conducted under visible light conditions with fluorescein as a photosensitizer. An outstanding improvement in the photocatalytic activity was achieved for the optimized sample (14.6 wt% MoS_2 loaded on TiO_2) with a hydrogen evolution rate of 10046 μmol·h^{-1}·g^{-1}. They concluded that this high performance of the MoS_2/TiO_2 composites is associated with the formation of active centers as well as the uniform distribution of MoS_2 and TiO_2 phases, inducing electrons' motion to reduce protons. In the proposed photocatalytic activity mechanism, excited electrons from fluorescein transfer to the CB of TiO_2. These electrons further move to the surface of MoS_2 and combine with protons to produce hydrogen. Liu and his coworker prepared MoS_2 nanosheets rooted in TiO_2 nanofibers (TiO_2@MoS_2) using a hydrothermal strategy [19]. They reported single- to few-layer MoS_2 nanosheets and TiO_2 nanofibers' porous structure. The MoS_2 nanosheets grew vertically on the porous structure of TiO_2, and deep rooting MoS_2 nanosheets into TiO_2 nanofibers put them in close contact for the electron transfer process and structural stability. The hydrogen production rates of the TiO_2@MoS_2 sample were 1.68 under UV–vis light and 0.49 mmol·h^{-1}·g^{-1} under visible light.

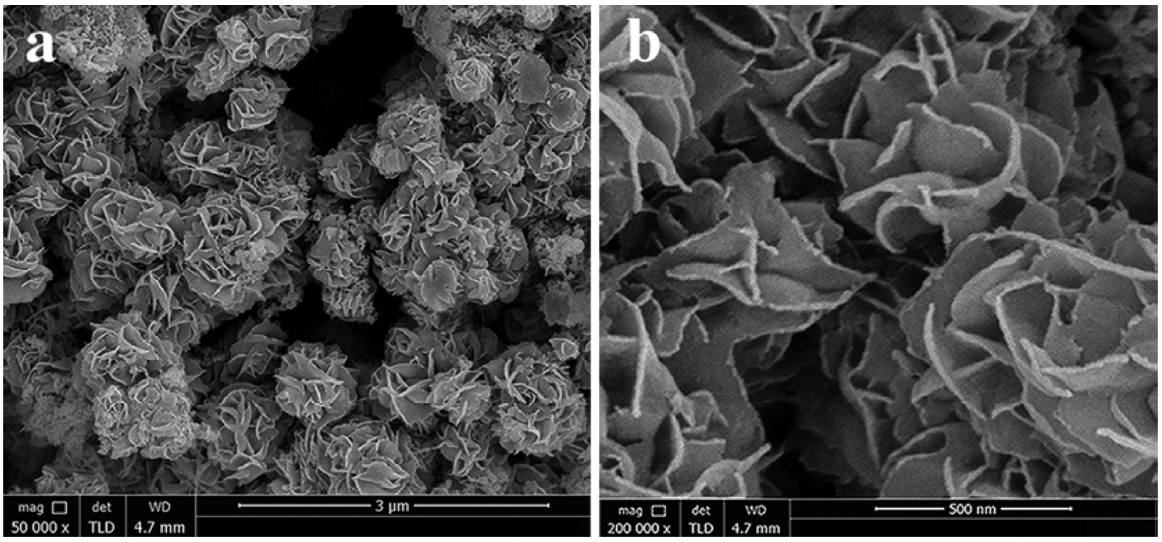

Figure 5. (**a**,**b**) SEM images of MoS_2@TiO_2 composites. Reprinted with permission from Ref. [77]. Copyright 2016 American Chemical Society.

TiO_2 nanomaterials combined with a MoS_2 co-catalyst can enhance hydrogen production rates up to several times.

5.2. MoS_2/Graphitic Carbon Nitride Composites

Graphitic carbon nitride (g-C_3N_4) is considered one of the promising candidates for photocatalysis due to its high chemical stability, environmentally friendly nature, and suitable energy bands that can efficiently absorb solar spectrum irradiation [78–81]. However, g-C_3N_4 suffers from a small specific surface area, high exciton binding energy, stacking back into a bulk, and low efficiency under visible light [82–84]. Recently, much interest has been devoted to g-C_3N_4-based composites for solar hydrogen production under visible light. To enhance the efficiency of its photocatalytic activity, various non-precious co-catalysts such as Co_2P, Mo_2C, and MoS_2 have been incorporated with C_3N_4 [85–87]. Among them, MoS_2 as a co-catalyst in MoS_2/C_3N_4 composites shows promising efficiency for photogenerated hydrogen production [87,88].

The design of and nano-interface coupling between MoS_2 and C_3N_4 can significantly enhance the photocatalytic HER performance. The appropriate MoS_2/C_3N_4 composites with an optimal ratio are believed to enhance solar absorption, increase the interfaces, and decrease the electron transfer distance of the photo-excited electrons between C_3N_4 and MoS_2 co-catalysts. Yuan's group reported MoS_2/g-C_3N_4 composites with various contents of MoS_2 developed using the solvent thermal method. The composite catalysts were evaluated for photocatalytic H_2 generation [87]. They found that MoS_2/g-C_3N_4 composites containing 0.75% MoS_2 nanosheets performed better and had a reaction rate of 1155 $\mu mol \cdot h^{-1} \cdot g^{-1}$ under visible light irradiation. The apparent quantum yield was about 6.8% under a monochromatic light of 420 nm. Furthermore, they explained that the large surface area of g-C_3N_4 nanosheets and the nano-interface coupling between MoS_2 nanosheets and g-C_3N_4 were mainly responsible for the outstanding photocatalytic hydrogen production of the MoS_2/g-C_3N_4 composite. Recently, Li et al., reported the in situ synthesis of a g-CN/MoS_2 composite [89]. The composite exhibited enhanced photocatalytic hydrogen production compared to pristine g-CN under visible light irradiation. The rod-like MoS_2 plays an important role as co-catalyst in the g-CN/MoS_2 composite in the enhancement of the hydrogen production rate. Zhang et al. reported sulfur-doped C_3N_4 with covalently crosslinked MoS_2 nanosheets (MoS_2/SC_3N_4) for improved photocatalytic hydrogen production [88]. The ultrathin array-like nanosheet structure of the MoS_2/SC_3N_3 composites was observed by SEM characterizations (see Figure 6). MoS_2/SC_3N_3 composites were studied for photocatalytic HER under visible light conditions. MoS_2/SC_3N_3 with 2.5%

MoS_2 nanosheets showed the optimal hydrogen production rate of 702.53 μmol·h^{-1}·g^{-1}. The array-like porous morphology had a rich exposed surface, covalent bonding structure, and enhanced visible light absorption by the cyano group of MoS_2/SC_3N_3 composites. This facilitates the photogenerated electrons' transfer from the CB of SC_3N_3 to MoS_2 via a heterojunction interface that consequently enhances the photocatalytic hydrogen evolution. Zhang et al. reported a $MoS_2/Fe_2O_3/g\text{-}C_3N_4$ ternary composite photocatalyst under hydrothermal conditions for hydrogen production [90]. The obtained ternary composite showed a hydrogen production rate about five times higher compared to $g\text{-}C_3N_4$. In addition, 1T MoS_2/C_3N_4 composites also show enhanced photocatalytic hydrogen production [91–94]. Li et al. loaded metallic 1T-phase MoS_2 quantum dots onto CdS nanorods (1T-MoS_2-CdS) using a one-step hydrothermal method at different temperatures [91]. The 1T-MoS_2-CdS composite prepared at 180 °C showed remarkable photocatalytic hydrogen production (131.7 mmol·h^{-1}·g^{-1}) under visible light (λ > 420 nm). This rate of hydrogen evolution reaction was over 65 times greater than that of pure CdS (mmol·h^{-1}·g^{-1}) and two times that of Pt-loaded CdS.

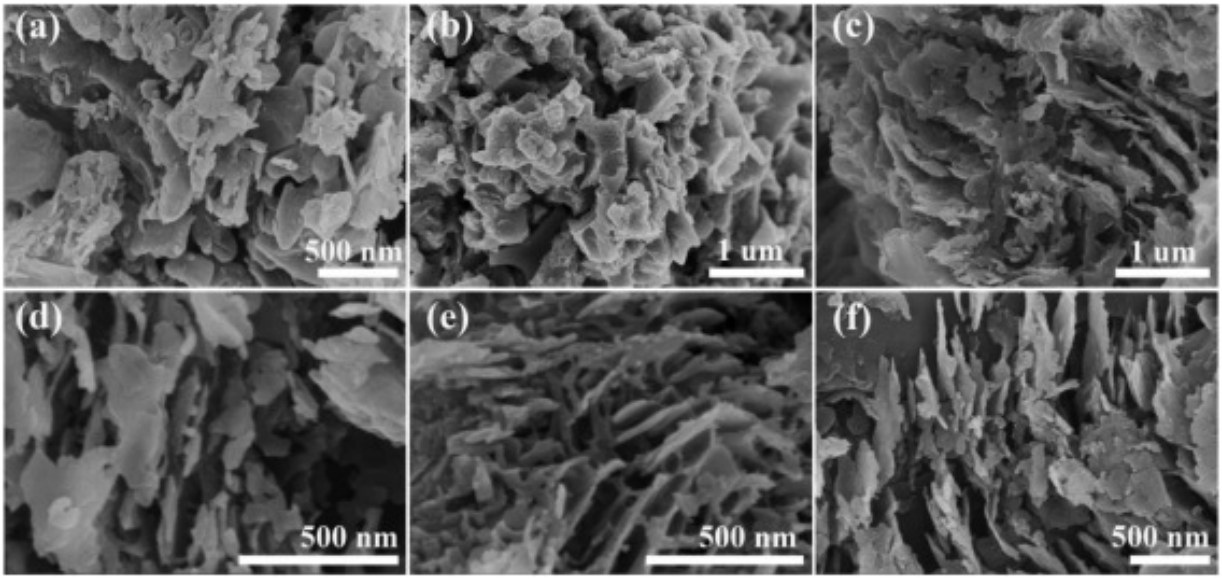

Figure 6. SEM images of (**a**) SC_3N_2, (**b**) MoS_2 and ultrathin array-like nanosheet, (**c**) MoS_2/SC_3N_4-0.5%, (**d**) MoS_2/SC_3N_4-1.5%, (**e**), MoS_2/SC_3N_4-2.5%, and (**f**) MoS_2/SC_3N_4-5.0%. Reprinted with permission from Ref. [88]. Copyright 2021 Elsevier.

Besides 1T-phase MoS_2, amorphous MoSx nanomaterials are efficient electrocatalysts as well as co-catalysts for hydrogen production [95–97]. They provide more unsaturated active S atoms, which can rapidly capture protons from the solution to convert them into hydrogen molecules. Yu et al. reported amorphous $MoSx/g\text{-}C_3N_4$ (a-$MoSx/g\text{-}C_3N_4$) composites developed using an adsorption in situ transformation method [95]. The a-$MoSx/g\text{-}C_3N_4$ composites were compared with crystalline $MoS_x/g\text{-}C_3N_4$ and $g\text{-}C_3N_4$ catalysts, and all of the a-$MoSx/g\text{-}C_3N_4$ catalysts displayed better photocatalytic performances than the crystalline $MoSx/g\text{-}C_3N_4$ and C_3N_4 catalysts. Among the a-$MoSx/g\text{-}C_3N_4$ composites, the a-$MoSx/g\text{-}C_3N_4$ catalyst with 3 wt% Mo showed the best photocatalytic performance and a hydrogen production rate of 273.1 μmol·h^{-1}·g^{-1}.

Similar to TiO_2/MoS_2 photocatalysts, $MoS_2/g\text{-}C_3N_4$ heterojunction composites can improve hydrogen production.

5.3. MoS_2 Coupling with Other Semiconductor Materials

As discussed earlier, MoS_2 as a co-catalyst for other semiconductor compounds can efficiently enhance the photocatalytic activity of hydrogen generation. The interfacial coupling of MoS_2 with semiconductor compounds has been designed in many strategies.

An appropriate ratio, increased interface area, and decreased migration distance of the photogenerated electrons between the MoS_2 and the semiconductor compounds can effectively improve photocatalytic hydrogen production. Zhang et al. reported MoS_2/CdS composites with willow branch-shaped morphology developed using a one-pot hydrothermal method [98]. The MoS_2/CdS composite with 5 wt% MoS_2 as a co-catalyst displayed an enhanced photocatalytic performance and produced 250.8 μmol·h^{-1} hydrogen evolution with an apparent quantum efficiency of 3.66% at 420 nm. Preparation of the willow branch-shaped nano-heterojunction morphology enhances the visible light absorption and also promotes the separation of photogenerated electron–hole pairs.

Ma et al. reported a layered CdS/MoS_2 heterostructure photocatalyst developed using ultrasonicated MoS_2 and CdS nanosheets, produced from hydro- and solvothermal methods, respectively [99]. When MoS_2 co-catalysts were loaded onto CdS nanosheets, the photocatalytic performance of the CdS/MoS_2 heterostructure was twice that of the pure CdS photocatalyst. The designing of a layered CdS/MoS_2 heterostructure could efficiently enhance the photogenerated charge separation and electron transfer, which improves the surface hydrogen evolution kinetics. Patriarchea and coworkers synthesized CdS nanoparticles using polymer-templated oxidative aggregation, and subsequently, MoS_2 nanosheets were deposited on it via the wet chemical method [100]. The obtained optimized MoS_2/CdS catalyst showed a good hydrogen production rate of about 0.4 mmol h^{-1} under visible light compared to the CdS catalyst. The enhanced hydrogen generation was due to the presence of the MoS_2 co-catalyst.

Samaniego-Benitez and coworkers prepared ZnS/MoS_2 heterostructure materials using a one-pot solvothermal method [101]. The hydrogen production yield of the ZnS/MoS_2 sample with 10% Mo reached 2600 μmol·h^{-1} under UV light for 4 h. They concluded that the enhanced photocatalytic activity was due to the synergistic effect between ZnS and MoS_2 and sulfur vacancies created in the ZnS structure during the synthesis process. In the proposed mechanism, a photoexcited electron moves from the CB of ZnS to the CB of MoS_2, where it interacts with the proton and produces hydrogen.

Recently, Guan et al., used MoS_2 as a co-catalyst for methylammonium lead iodide to split hydrogen iodide for photocatalytic HER [102]. The methylammonium lead iodide microcrystals and MoS_2 nanoflowers ($MAPbI_3$/MoS_2) formed a heterostructure. The MoS_2 nanoflowers have plenty of active catalyst sites for hydrogen evolution. The hydrogen evolution rate of $MAPbI_3$/MoS_2 reached ~30,000 μmol·h^{-1}·g^{-1} and a solar-derived hydrogen iodide splitting efficiency of 7.35% was achieved under visible light irradiation. This hydrogen evolution rate is more than 1000 times higher compared to that of pristine $MAPbI_3$. The MoS_2 can induce charge separation and provide abundant active sites for photocatalytic hydrogen evolution.

For these examples, we can conclude that MoS_2 is an efficient co-catalyst for CdS, ZnS, and $MAPbI_3$ etc, catalysts to produce hydrogen.

5.4. MoS_2 and Other Co-Catalyst Heterojunction Composites

The heterojunction of a MoS_2 co-catalyst with other co-catalysts is an attractive strategy because it can improve the photogenerated electron transfer from a semiconductor to a MoS_2 co-catalyst during photocatalysis, which enhances the activity via the catalytic sites on MoS_2 co-catalysts [103–105]. The heterojunctions between MoS_2 and highly conductive co-catalysts decrease the resistance effect and increase the electron transfer process during photocatalysis [106].

For improved photocatalytic H_2 evolution, a widely studied example of anchoring a MoS_2 co-catalyst on graphene has been reported [107,108]. Xiang et al., synthesized a TiO_2/MoS_2/graphene hybrid photocatalyst for hydrogen production [18]. The hybrid photocatalyst showed significant enhancement of photocatalytic H_2 generation under UV illumination, with an apparent quantum efficiency of 9.7% at 365 nm. The improved activity is described in terms of synergetic effects between MoS_2 and the conductive graphene co-catalysts and TiO_2 leading to outstanding photocatalytic hydrogen evolution activity.

These authors have proposed a mechanism for the significant boost of photocatalytic H_2 generation. They reported that this enhancement is due to the transfer of photogenerated electrons from the CB of TiO_2 nanoparticles to the CB of MoS_2 nanosheets through highly conductive graphene sheets (Figure 7), where H^+ ions are adsorbed at an active site of MoS_2. Apart from graphene, other highly conductive materials such as metal sulfides and phosphides can also be used as interfacial electron transfer sources to enhance photocatalytic hydrogen evolution. Lu and coworkers synthesized g-C_3N_4, Ni_2P, and MoS_2 heterojunctions by hydrothermal and ultrasonic methods [109]. The hydrogen production rate of the g-C_3N_4-1%Ni_2P-1.5%MoS_2 composite was about 532.41 $\mu mol \cdot h^{-1} \cdot g^{-1}$ under visible light, which is 5.15- and 2.47-fold higher than those of g-C_3N_4-1%Ni_2P and g-C_3N_4-1.5%MoS_2, respectively. The Ni_2P co-catalyst could be acting as an interface electron bridge between g-C_3N_4 and MoS_2 nanosheets. It provides interfacial electron transfer channels in g-C_3N_4/MoS_2 heterostructure composites and prevents the rapid recombination process of photogenerated charge carriers.

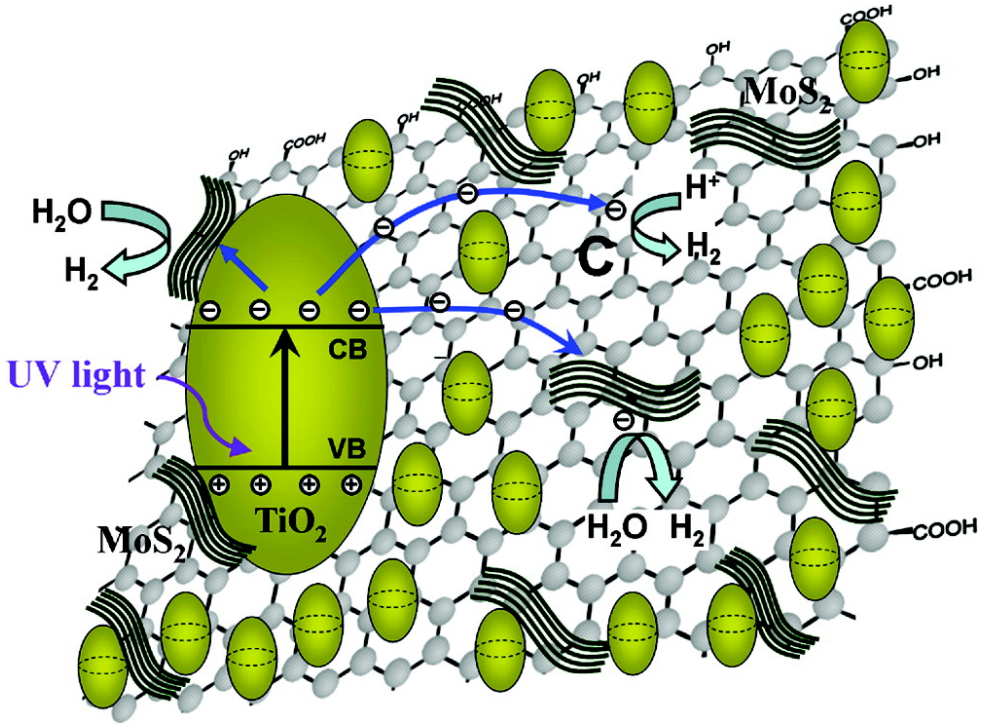

Figure 7. Schematic illustration of the charge transfer and proposed mechanism of electron transfer in TiO_2/MoS_2/graphene composites. Reprinted with permission from Ref. [18]. Copyright 2012 American Chemical Society.

Finally, we summarize some heterojunction composites with semiconducting and MoS_2 materials in which the MoS_2 nanomaterial acts as a co-catalyst for enhanced photocatalytic hydrogen production. Table 1 and Figure 8 show different strategies used for various types of catalysts combined with a MoS_2 co-catalyst to form heterojunction composites for enhanced photocatalytic hydrogen production.

Table 1. Summary of MoS_2 usage as a co-catalyst for various materials to form heterostructures for photocatalytic hydrogen generation.

Catalyst	Synthesis Method	Light Source	Photocatalytic Activity	No. of Cycles	Total Times of Cycles (h)	Ref.
MoS_2 nanoparticles/TiO_2 nanoparticles	Mechanochemistry	300 W Xe lamp (λ = 250–380 nm)	150.7 $\mu mol \cdot h^{-1} \cdot g^{-1}$	3	18	[76]
TiO_2 nanofibers @MoS_2 nanosheets	Hydrothermal	300 W xenon lamp λ > 320 nm or λ > 420 nm	1.68 $mmol \cdot h^{-1} \cdot g^{-1}$ 0.49 $mmol \cdot h^{-1} \cdot g^{-1}$	6	30	[19]
Flower-like MoS_2@TiO_2 nanohybrids	Metal organic framework-derived	300 W Xe lamp (λ ≥ 420 nm)	10046 $\mu mol \cdot h^{-1} \cdot g^{-1}$	3	10	[77]
MoS_2 nanosheets/TiO_2 nanotubes	Hydrothermal process	300 W Xe-lamp (λ ≥ 420 nm)	143.32 $\mu mol \cdot h^{-1} \cdot g^{-1}$	4	14	[110]
MoS_2 nanosheets/g-C_3N_4 nanosheets	Solvothermal method	300 W Xe-lamp (λ > 420 nm	1155 $\mu mol \cdot h^{-1} \cdot g^{-1}$	3	12	[87]
S-doped C_3N_4 nanosheets/MoS_2 nanosheets	One-step solid-state strategy	Visible LED lamp	702.53 $\mu mol \cdot h^{-1} \cdot g^{-1}$	3	16	[88]
Amorphous MoS_x nanoparticles/g-C_3N_4 nanosheets	Adsorption in situ transformation method	Low-power LEDs (3W, 420 nm)	273.1 $\mu mol \cdot h^{-1} \cdot g^{-1}$	4	12	[95]
g-C_3N_4/NCDS/MoS_2	Thermal polymerization and solvothermal approach	300 W Xe lamp (λ ≥ 420 nm)	212.41 $\mu mol \cdot h^{-1} \cdot g^{-1}$	4	16	[111]
ZnS/MoS_2 particles	One-pot solvothermal	Hg pen-lamp (254 nm), (4.4 mW/cm^2)	606 $\mu mol \cdot h^{-1} \cdot g^{-1}$	-	-	[101]
MoS_2 clusters/CdS nanorod	Solvothermal method	300 W Xe lamp (λ ≥ 420 nm)	12.38 $mmol \cdot h^{-1} \cdot g^{-1}$	4		[112]
MoS_2/$ZnIn_2S_4$ microspheres	Impregnation method	300 W Xe-lamp (λ > 420 nm)	3.06 $mmol \cdot h^{-1} \cdot g^{-1}$	3	15	[113]
MoS_2 nanosheets/$ZnIn_2S_4$ microspheres	In situ photo-assisted deposition	300 W Xe-lamp (λ > 420 nm)	8.047 $mmol \cdot h^{-1} \cdot g^{-1}$	-	-	[114]
MoS_2 nanoflake-$Mn_{0.2}Cd_{0.8}S$ nanorod/MnS nanoparticle	One-pot solvothermal	300 W Xe lamp (λ ≥ 420 nm)	995 $\mu mol \cdot h^{-1}$	5	20	[115]

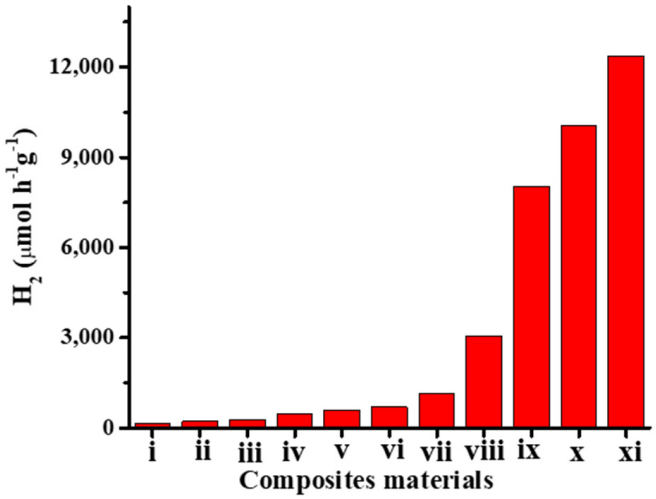

Figure 8. Photocatalytic hydrogen production of heterojunction materials using MoS_2 as a co-catalyst. (i) MoS_2 nanosheets/TiO_2 nanotubes [110]. (ii) g-C_3N_4/NCDS/MoS_2 [111]. (iii) Amorphous MoS_x nanoparticles/g-C_3N_4 nanosheets [95]. (iv) TiO_2 nanofibers/@MoS_2 nanosheets [19]. (v) ZnS/MoS_2 particles [101]. (vi) S-doped C_3N_4 nanosheets/MoS_2 nanosheets [88]. (vii) MoS_2 nanosheets/g-C_3N_4 nanosheets [87]. (viii) MoS_2/$ZnIn_2S_4$ microspheres [113]. (ix) MoS_2 nanosheets/$ZnIn_2S_4$ microspheres [114]. (x) Flower-like MoS_2@TiO_2 nanohybrids [77]. (xi) MoS_2 clusters/CdS nanorod [112].

6. Conclusions and Outlook

In summary, we highlighted the significance of MoS_2 as a co-catalyst to improve hydrogen evolution. A comprehensive analysis of the literature led us to conclude that MoS_2 is a good co-catalyst for other semiconducting materials such as TiO_2, C_3N_4, CdS, ZnS, etc., which form heterostructure nanocomposites and consequently boost the photocatalytic hydrogen generation ability. However, there are still some critical issues that must be resolved, such as the downsizing of MoS_2 nanosheets for appropriate band gap alignment and the high density of catalytic active sites. These issues can be solved by reducing the size of MoS_2 to quantum dots or the molecular level, which will certainly enhance the catalytic active sites. The photoexcited electron transfers between photocatalysts and the MoS_2 co-catalyst play an important role during photocatalytic hydrogen generation. The electron transfer mechanism at the interface of a semiconductor photocatalyst and a MoS_2 co-catalyst is yet to be fully investigated and completely understood. It is important to conduct theoretical studies such as density functional theory (DFT) simulations and apply in situ testing methods to understand electron transfer paths. Although MoS_2 nanosheets as a co-catalyst are a promising candidate for photocatalytic hydrogen production, all the challenges require further efforts and study.

Author Contributions: Conceptualization and validation, S.A.S., I.K. and A.Y.; writing—original draft preparation, S.A.S. and I.K.; writing—review and editing, S.A.S. and A.Y.; supervision, A.Y. All authors have read and agreed to the published version of the manuscript.

Funding: This research received no external funding.

Institutional Review Board Statement: Not Applicable.

Informed Consent Statement: Not Applicable.

Data Availability Statement: No supporting data is reported.

Acknowledgments: We are thankful to the National Natural Science Foundation of China (under research grant no. 22150410332) and the start-up foundation for the introduction of talent at Jiangsu University of Science and Technology, China.

Conflicts of Interest: The authors declare no conflict of interest.

References

1. Kampouri, S.; Stylianou, K.C. Dual-functional photocatalysis for simultaneous hydrogen production and oxidation of organic substances. *ACS Catal.* **2019**, *9*, 4247–4270. [CrossRef]
2. Wang, Q.; Domen, K. Particulate photocatalysts for light-driven water splitting: Mechanisms, challenges, and design strategies. *Chem. Rev.* **2020**, *120*, 919–985. [CrossRef] [PubMed]
3. Sanchez-Bastardo, N.; Robert, S.; Ruland, H. Methane pyrolysis for zero-Emission hydrogen production: A potential bridge technology from fossil fuels to a renewable and sustainable hydrogen economy. *Ind. Eng. Chem. Res.* **2021**, *60*, 11855–11881. [CrossRef]
4. Shah, S.A.; Shen, X.; Yuan, A.; Ji, Z.; Yue, X.; Zhu, G.; Zhou, H.; Xu, K.; Zhu, J.; Chen, Y. One step in-situ synthesis of Ni_3S_2/Fe_2O_3/N-doped carbon composites on Ni foam as an efficient electrocatalyst for overall water splitting. *Appl. Surf. Sci.* **2020**, *527*, 146918. [CrossRef]
5. Ola, O.; Ullah, H.; Chen, Y.; Thummavichai, K.; Wang, N.; Zhu, Y. DFT and experimental studies of iron oxide-based nanocomposites for efficient electrocatalysis. *J. Mater. Chem. C* **2021**, *9*, 6409–6417. [CrossRef]
6. Wang, Z.; Li, C.; Domen, K. Recent developments in heterogeneous photocatalysts for solar-driven overall water splitting. *Chem. Soc. Rev.* **2019**, *48*, 2109–2125. [CrossRef]
7. Zhao, H.; Jiang, Z.; Xiao, K.; Sun, H.; Chan, H.S.; Tsang, T.H.; Yang, S.; Wong, P.K. Photo-assisted separation of noble-metal-free oxidation and reduction cocatalysts for graphitic carbon nitride nanosheets with efficient photocatalytic hydrogen evolution. *Appl. Catal. B-Environ.* **2021**, *280*, 119456. [CrossRef]
8. Fujishima, A.; Honda, K. Electrochemical photolysis of water at a semiconductor electrode. *Nature* **1972**, *238*, 37–38. [CrossRef]
9. Wen, J.; Li, X.; Liu, W.; Fang, Y.; Xie, J.; Xu, Y. Strategies for engineering metal-organic frameworks as efficient photocatalysts. *Chin. J. Catal.* **2015**, *36*, 2049–2070. [CrossRef]
10. Kong, D.; Fan, H.; Yin, D.; Zhang, D.; Pu, X.; Yao, S.; Su, C. $AgFeO_2$ Nanoparticle/$ZnIn_2S_4$ Microsphere p–n heterojunctions with hierarchical nanostructures for efficient visible-light-driven H_2 evolution. *ACS Sustain. Chem. Eng.* **2021**, *9*, 2673–2683. [CrossRef]
11. Mahler, B.; Hoepfner, V.; Liao, K.; Ozin, G.A. Colloidal synthesis of 1T-WS_2 and 2H-WS_2 nanosheets: Applications for photocatalytic hydrogen evolution. *J. Am. Chem. Soc.* **2014**, *136*, 14121–14127. [CrossRef] [PubMed]
12. Li, Y.; Ding, L.; Yin, S.; Liang, Z.; Xue, Y.; Wang, X.; Cui, H.; Tian, J. Photocatalytic H_2 Evolution on TiO_2 Assembled with Ti_3C_2 MXene and Metallic 1T-WS_2 as Co-catalysts. *Nano-Micro Lett.* **2020**, *12*, 6. [CrossRef] [PubMed]
13. Dai, C.; Liu, B. Conjugated polymers for visible-light-driven photocatalysis. *Energy Environ. Sci.* **2020**, *13*, 24. [CrossRef]
14. Wan, Y.; Deng, J.; Gu, C.; Ma, Y. Highly efficient photocatalytic hydrogen evolution based on conjugated molecular micro/nanocrystalline sheets. *J. Mater. Chem. A* **2021**, *9*, 2120. [CrossRef]
15. Luo, L.; Gong, Z.; Ma, J.; Wang, K.; Zhu, H.; Li, K.; Xiong, L.; Guo, X.; Tang, J. Ultrathin sulfur-doped holey carbon nitride nanosheets with superior photocatalytic hydrogen production from water. *Appl. Catal. B-Environ.* **2021**, *284*, 119742. [CrossRef]
16. Sun, K.; Liu, M.; Pei, J.; Li, D.; Ding, C.; Wu, K.; Jiang, H. Incorporating transition-metal phosphides into metal-organic frameworks for enhanced photocatalysis. *Angew. Chem. Int. Ed.* **2020**, *59*, 22749. [CrossRef]
17. Chen, W.; Wang, L.; Mo, D.; He, F.; Wen, Z.; Wu, X.; Xu, H.; Chen, L. Modulating benzothiadiazole-based covalent organic frameworks via halogenation for enhanced photocatalytic water splitting. *Angew. Chem. Int. Ed.* **2020**, *59*, 16902. [CrossRef]
18. Xiang, Q.; Yu, J.; Jaroniec, M. Synergetic effect of MoS_2 and graphene as cocatalysts for enhanced photocatalytic H_2 production activity of TiO_2 nanoparticles. *J. Am. Chem. Soc.* **2012**, *134*, 6575–6578. [CrossRef]
19. Liu, C.; Wang, L.; Tang, Y.; Luo, S.; Liu, Y.; Zhang, S.; Zeng, Y.; Xu, Y. Vertical single or few-layer MoS_2 nanosheets rooting into TiO_2 nanofibers for highly efficient photocatalytic hydrogen evolution. *Appl. Catal. B-Environ.* **2015**, *164*, 1–9. [CrossRef]
20. Shah, S.A.; Xu, L.; Sayyar, R.; Bian, T.; Liu, Z.; Yuan, A.; Shen, X.; Khan, I.; Tahir, A.A.; Ullah, H. Growth of MoS_2 nanosheets on M@N-doped carbon particles (M = Co, Fe or CoFe Alloy) as an efficient electrocatalyst toward hydrogen evolution reaction. *Chem. Eng. J.* **2022**, *428*, 132126. [CrossRef]
21. Wilcoxon, J.P.; Newcomer, P.P.; Samara, G.A. Synthesis and optical properties of MoS_2 and isomorphous nanoclusters in the quantum confinement regime. *J. Appl. Phys.* **1997**, *81*, 7934. [CrossRef]
22. Thurston, T.R.; Wilcoxon, J.P. Photooxidation of organic chemicals catalyzed by nanoscale MoS_2. *J. Phys. Chem. B* **1999**, *103*, 11–17. [CrossRef]
23. Liu, H.; Li, Y.; Xiang, M.; Zeng, H.; Shao, X. Single-layered MoS_2 directly grown on rutile TiO_2 (110) for enhanced interfacial charge transfer. *ACS Nano* **2019**, *13*, 6083–6089. [CrossRef] [PubMed]
24. Li, Z.; Meng, X.; Zhang, Z. Recent development on MoS_2-based photocatalysis: A review. *J. Photochem. Photobiol. C* **2018**, *35*, 39–55. [CrossRef]
25. Khalila, R.M.A.; Hussaina, F.; Rana, A.M.; Imran, M.; Murtaza, G. Comparative study of polytype 2H-MoS_2 and 3R-MoS_2 systems by employing DFT. *Phys. E Low-Dimens. Syst. Nanostruct.* **2019**, *106*, 338–345. [CrossRef]
26. Samanian, M.; Ghatee, M.H. Study of the molybdenum dichalcogenide crystals: Recent developments and novelty of the P-MoS_2 structure. *J. Mol. Model.* **2021**, *27*, 268. [CrossRef]
27. Eidsavg, H.; Rasukkannu, M.; Velauthapillai, D.; Vajeeston, P. In-depth first-principle study on novel MoS_2 polymorphs. *RSC Adv.* **2021**, *11*, 3759–3769. [CrossRef]
28. Wang, Q.H.; Kalantar-Zadeh, K.; Kis, A.; Coleman, J.N.; Strano, M.S. Electronics and optoelectronics of two-dimensional transition metal dichalcogenides. *Nat. Nanotechnol.* **2012**, *7*, 699–712. [CrossRef]

29. Liang, Z.; Shen, R.; Ng, Y.H.; Zhang, P.; Xiang, Q.; Li, X. A review on 2D MoS_2 cocatalysts in photocatalytic H_2 production. *J. Mater. Sci. Technol.* **2020**, *56*, 89–121. [CrossRef]
30. Acerce, M.; Voiry, D.; Chhowalla, M. Metallic 1T phase MoS_2 nanosheets as supercapacitor electrode materials. *Nat. Nanotechnol.* **2015**, *10*, 313–318. [CrossRef]
31. Cheng, P.; Sun, K.; Hu, Y.H. Memristive Behavior and Ideal Memristor of 1T Phase MoS_2 Nanosheets. *Nano Lett.* **2016**, *16*, 572–576. [CrossRef] [PubMed]
32. Mak, K.F.; Lee, C.; Hone, J.; Shan, J.; Heinz, T.F. Atomically Thin MoS_2: A new direct-gap semiconductor. *Phys. Rev. Lett.* **2010**, *105*, 136805. [CrossRef] [PubMed]
33. Kuc, A.; Zibouche, N.; Heine, T. Influence of quantum confinement on the electronic structure of the transition metal sulfide TS_2. *Phys. Rev. B* **2011**, *83*, 245213. [CrossRef]
34. Su, L.; Luo, L.L.; Wang, J.W.; Song, T.; Tu, W.X.; Wang, Z.J. Lamellar flower-like porous MoS_2 as an efficient cocatalyst to boost photocatalytic hydrogen evolution of CdS. *Catal. Sci. Technol.* **2021**, *11*, 1292–1297. [CrossRef]
35. Zhang, S.; Duan, S.; Chen, G.; Meng, S.; Zheng, X.; Fan, Y.; Fu, X.; Chen, S. $MoS_2/Zn_3In_2S_6$ composite photocatalysts for enhancement of visible light-driven hydrogen production from formic acid. *Chin. J. Catal.* **2021**, *42*, 193–204. [CrossRef]
36. Sun, J.; Yin, M.; Li, Y.; Liang, K.; Fan, Y.; Li, Z. Efficient photocatalytic hydrogen production of ternary composite constituted by cubic CdS, MoS_2 and activated carbon. *J. Alloys Compd.* **2021**, *874*, 59930. [CrossRef]
37. Sun, J.; Duan, L.; Wu, Q.; Yao, W. Synthesis of MoS_2 quantum dots cocatalysts and their efficient photocatalytic performance for hydrogen evolution. *Chem. Eng. J.* **2018**, *332*, 449–455. [CrossRef]
38. Lee, G.J.; Chen, H.C.; Wu, J.J. (In, Cu) Co-doped ZnS nanoparticles for photoelectrochemical hydrogen production. *Int. J. Hydrogen Energy* **2019**, *44*, 110–117. [CrossRef]
39. Jeong, S.Y.; Song, J.; Lee, S. Photoelectrochemical device designs toward practical solar water splitting: A review on the recent progress of $BiVO_4$ and $BiFeO_3$ photoanodes. *Appl. Sci.* **2018**, *8*, 1388. [CrossRef]
40. Zhou, K.G.; Mao, N.N.; Wang, H.X.; Peng, Y.; Zhang, H.L. A mixed-solvent strategy for efficient exfoliation of inorganic graphene analogues. *Angew. Chem. Int. Ed.* **2011**, *50*, 10839–10842. [CrossRef]
41. Li, H.; Yin, Z.; He, Q.; Li, H.; Huang, X.; Lu, G.; Fam, D.W.; Tok, A.I.; Zhang, Q.; Zhang, H. Fabrication of single- and multilayer MoS_2 film-based field-effect transistors for sensing NO at room temperature. *Small* **2012**, *8*, 63–67. [CrossRef] [PubMed]
42. Hu, D.; Xiang, J.; Zhou, Q.W.; Su, S.Q.; Zhang, Z.B.; Wang, X.; Jin, M.L.; Nian, L.; Nozel, R.; Zhou, G.F.; et al. One-step chemical vapor deposition of MoS_2 nanosheets on SiNWs as photocathodes for efficient and stable solar-driven hydrogen production. *Nanoscale* **2018**, *10*, 3518–3525. [CrossRef] [PubMed]
43. Huang, T.; Chen, W.; Liu, T.Y.; Hao, Q.L.; Liu, X.H. Hybrid of AgInZnS and MoS_2 as efficient visible-light driven photocatalyst for hydrogen production. *Int. J. Hydrogen Energy* **2017**, *42*, 12254–12261. [CrossRef]
44. Wei, J.; Huang, H.; Luo, Q.; Liu, N.; Wang, X.Y.; Wang, X.F.; Zhong, M.; Huang, X.L. Synthesis of few layers amorphous 1T/2H MoS_2 by a one-step ethanol/water solvothermal method and its hydrodesulfurization performance. *Catal. Lett.* **2022**, *152*, 263–275. [CrossRef]
45. Yang, Y.; Liu, Z.; Shu, K.; Li, L.; Li, J. Improved performances of CVD-grown MoS_2 based phototransistors enabled by encapsulation. *Adv. Mater. Interfaces* **2021**, *8*, 2100164. [CrossRef]
46. Li, H.; Wu, J.; Yin, Z.; Zhang, H. Preparation and applications of mechanically exfoliated single-layer and multilayer MoS_2 and WSe_2 nanosheets. *Acc. Chem. Res.* **2014**, *47*, 1067–1075. [CrossRef]
47. Jeon, J.; Lee, J.; Yoo, G.; Park, J.H.; Yeom, G.Y.; Jang, Y.H.; Lee, S. Size-tunable synthesis of monolayer MoS_2 nanoparticles and their applications in non-volatile memory devices. *Nanoscale* **2016**, *8*, 16995–17003. [CrossRef]
48. Zhang, S.; Liu, X.; Liu, C.; Luo, S.; Wang, L.; Cai, T.; Zeng, Y.; Yuan, J.; Dong, W.; Pei, Y.; et al. MoS_2 quantum dots growth induced by S vacancy in $ZnIn_2S_4$ monolayer: Atomic-level heterostructure for photocatalytic hydrogen production. *ACS Nano* **2018**, *12*, 751–758. [CrossRef]
49. Huang, Y.; Pan, Y.H.; Yang, R.; Bao, L.H.; Meng, L.; Luo, H.L.; Cai, Y.Q.; Liu, G.D.; Zhao, W.J.; Zhou, Z.; et al. Universal mechanical exfoliation of large-area 2D crystals. *Nat. Commun.* **2020**, *11*, 2453. [CrossRef]
50. Eda, G.; Yamaguchi, H.; Voiry, D.; Fujita, T.; Chen, M.; Chhowalla, M. Photoluminescence from chemically exfoliated MoS_2. *Nano Lett.* **2011**, *11*, 5111–5116. [CrossRef]
51. Ambrosi, A.; Pumera, M. Electrochemical exfoliation of MoS_2 crystal for hydrogen electrogeneration. *Chem. Eur. J.* **2018**, *24*, 18551–18555. [CrossRef] [PubMed]
52. Liu, Y.; He, X.; Hanlon, D.; Harvey, A.; Coleman, J.N.; Li, Y. Liquid phase exfoliated MoS_2 nanosheets percolated with carbon nanotubes for high volumetric/areal capacity sodium-ion batteries. *ACS Nano* **2016**, *10*, 8821–8828. [CrossRef] [PubMed]
53. Ottaviano, L.; Palleschi, S.; Perrozzi, F.; DOlimpio, G.; Priante, F.; Donarelli, M.; Benassi, P.; Nardone, M.; Gonchigsuren, M.; Gombosuren, M.; et al. Mechanical exfoliation and layer number identification of MoS_2 revisited. *2D Mater.* **2017**, *4*, 045013. [CrossRef]
54. Zhang, H. Ultrathin two-dimensional nanomaterials. *ACS Nano* **2015**, *9*, 9451–9469. [CrossRef] [PubMed]
55. Magda, G.; Peto, J.; Dobrik, G.; Hwang, C.; Biro, L.P.; Tapaszto, L. Exfoliation of large-area transition metal chalcogenide single layers. *Sci. Rep.* **2015**, *5*, 14714. [CrossRef]
56. Desai, S.B.; Madhvapathy, S.R.; Amani, M.; Kiriya, D.; Hettick, M.; Tosun, M.; Zhou, Y.; Dubey, M.; Ager, J.W.; Chrzan, D.; et al. Gold-mediated exfoliation of ultralarge optoelectronically-perfect monolayers. *Adv. Mater.* **2016**, *28*, 4053–4058. [CrossRef]

57. Velicky, M.; Donnelly, G.E.; Hendren, W.R.; McFarland, S.; Scullion, D.; DeBenedetti, W.J.I.; Correa, G.C.; Han, Y.; Wain, A.J.; Hines, M.A.; et al. Mechanism of Gold-assisted exfoliation of centimeter-sized transition-metal dichalcogenide monolayers. *ACS Nano* **2018**, *12*, 10463–10472. [CrossRef]
58. Lin, Y.C.; Zhang, W.; Huang, J.K.; Liu, K.K.; Lee, Y.H.; Liang, C.T.; Chu, C.W.; Li, L.J. Wafer-scale MoS_2 thin layers prepared by MoO_3 sulfurization. *Nanoscale* **2012**, *4*, 6637–6641. [CrossRef]
59. Cai, J.; Jian, J.; Chen, X.; Lei, M.; Wang, W. Regular hexagonal MoS_2 microflakes grown from MoO_3 precursor. *Appl. Phys. A* **2007**, *89*, 783–788. [CrossRef]
60. Zhan, Y.; Liu, Z.; Najmaei, S.; Ajayan, P.; Lou, J. Large-area vapor-phase growth and characterization of MoS_2 atomic layers on a SiO_2 substrate. *Small* **2014**, *8*, 966–971. [CrossRef]
61. Song, I.; Park, C.; Hong, M.; Baik, J.; Shin, H.-J.; Choi, H. Patternable large-scale molybdenium disulfide atomic layers grown by gold-assisted chemical vapor deposition. *Angew. Chem. Int. Ed.* **2014**, *53*, 1266–1269. [CrossRef] [PubMed]
62. Ahn, C.; Lee, J.; Kim, H.-U.; Bark, H.; Jeon, M.; Ryu, G.; Lee, Z.; Yeom, G.; Kim, K.; Jung, J.; et al. Low-temperature synthesis of large-scale molybdenum disulfide thin films directly on a plastic substrate using plasma-enhanced chemical vapor deposition. *Adv. Mater.* **2015**, *27*, 5223–5229. [CrossRef] [PubMed]
63. Kang, K.; Xie, S.; Huang, L.; Han, Y.; Huang, P.; Mak, K.; Kim, C.-J.; Muller, D.; Park, J. High-mobility three-atom-thick semiconducting films with wafer-scale homogeneity. *Nature* **2015**, *520*, 656–660. [CrossRef] [PubMed]
64. Kumar, V.; Dhar, S.; Choudhury, T.; Shivashankar, S.; Raghavan, S. A predictive approach to CVD of crystalline layers of TMDs: The case of MoS_2. *Nanoscale* **2015**, *7*, 7802–7810. [CrossRef]
65. Vishwanath, S.; Liu, X.; Rouvimov, S.; Mende, P.; Azcatl, A.; McDonnell, S.; Wallace, R.; Feenstra, R.; Furdyna, J.; Jena, D.; et al. Comprehensive structural and optical characterization of MBE grown $MoSe_2$ on graphite, CaF_2 and graphene. *2D Mater.* **2015**, *2*, 024007. [CrossRef]
66. Qin, X.; Ke, P.; Wang, A.; Kim, K. Microstructure, mechanical and tribological behaviors of MoS_2-Ti composite coatings deposited by a hybrid HIPIMS method. *Surf. Coat. Technol.* **2013**, *228*, 275–281. [CrossRef]
67. Feng, X.; Tang, Q.; Zhou, J.; Fang, J.; Ding, P.; Sun, L.; Shi, L. Novel mixed–solvothermal synthesis of MoS_2 nanosheets with controllable morphologies. *Cryst. Res. Technol.* **2013**, *48*, 363–368. [CrossRef]
68. Liu, Y.; Xu, X.; Li, H.; Si, Z.; Wu, X.; Ra, R.; Duan, W. A facile one step synthesis of MoS_2/g-C_3N_4 photocatalyst with enhanced visible light photocatalytic hydrogen production. *Catal. Lett.* **2022**, *152*, 972–979. [CrossRef]
69. Deng, Z.; Hu, Y.; Ren, D.; Lin, S.; Jiang, H.; Li, C. Reciprocal hybridization of MoO_2 nanoparticles and few-layer MoS_2 for stable lithium-ion batteries. *Chem. Commun.* **2015**, *51*, 13838–13841. [CrossRef]
70. Jagminas, A.; Naujokaitis, A.; Gaigalas, P.; Ramanavicius, S.; Kurtinaitiene, M.; Trusovas, R. Substrate impact on the structure and electrocatalyst properties of molybdenum disulfide for HER from water. *Metals* **2020**, *10*, 1251. [CrossRef]
71. Guo, X.; Wang, Z.; Zhu, W.; Yang, H. The novel and facile preparation of multilayer MoS_2 crystals by a chelation-assisted sol-gel method and their electrochemical performance. *RSC Adv.* **2017**, *7*, 9009–9014. [CrossRef]
72. Shah, S.A.; Shen, X.; Xie, M.; Zhu, G.; Ji, Z.; Zhou, H.; Xu, K.; Yue, X.; Yuan, A.; Zhu, J.; et al. Nickel@nitrogen-doped carbon@MoS_2 nanosheets: An efficient electrocatalyst for hydrogen evolution reaction. *Small* **2019**, *15*, 1804545. [CrossRef] [PubMed]
73. Shah, S.A.; Zhu, G.; Shen, X.; Kong, L.; Ji, Z.; Xu, K.; Zhou, H.; Zhu, J.; Song, P.; Song, C.; et al. Controllable sandwiching of reduced graphene oxide in hierarchical defect-rich MoS_2 ultrathin nanosheets with expanded interlayer spacing for electrocatalytic hydrogen evolution reaction. *Adv. Mater. Interfaces* **2018**, *5*, 1801093. [CrossRef]
74. Zhu, J.; Zhu, S.; Kong, X.; Liang, Y.; Li, Z.; Wu, S.; Luo, S.; Chang, C.; Cui, Z. Rutile-coated B-phase TiO_2 heterojunction nanobelts for photocatalytic H_2 evolution. *ACS Appl. Nano Mater.* **2020**, *3*, 10349–10359. [CrossRef]
75. Yang, W.; Li, M.; Pan, K.; Guo, L.; Wu, J.; Li, Z.; Yang, F.; Lin, K.; Zhou, W. Surface engineering of mesoporous anatase titanium dioxide nanotubes for rapid spatial charge separation on horizontal-vertical dimensions and efficient solar-driven photocatalytic hydrogen evolution. *J. Colloid Interface Sci.* **2021**, *586*, 75–83. [CrossRef]
76. Zhu, Y.; Ling, Q.; Liu, Y.; Wang, H.; Zhu, Y. Photocatalytic H_2 evolution on MoS_2-TiO_2 catalysts synthesized via mechanochemistry. *Phys. Chem. Chem. Phys.* **2015**, *17*, 933–940. [CrossRef]
77. Ma, B.; Guan, P.Y.; Li, Q.Y.; Zhang, M.; Zang, S.Q. MOF derived flower-like MoS_2@TiO_2 nanohybrids with enhanced activity for hydrogen evolution. *ACS Appl. Mater. Interfaces* **2016**, *8*, 26794–26800. [CrossRef]
78. Zhou, Z.; Zhang, Y.; Shen, Y.; Liu, S.; Zhang, Y. Molecular engineering of polymeric carbon nitride: Advancing applications from photocatalysis to biosensing and more. *Chem. Soc. Rev.* **2018**, *47*, 2298–2321. [CrossRef]
79. Khan, I.; Luo, M.; Guo, L.; Khan, S.; Shah, S.A.; Khan, I.; Khan, A.; Wang, C.; Ai, B.; Zaman, S. Synthesis of phosphate-bridged g-C_3N_4/$LaFeO_3$ nanosheets Z-scheme nanocomposites as efficient visible photocatalysts for CO_2 reduction and malachite green degradation. *Appl. Catal. A Gen.* **2022**, *629*, 118418. [CrossRef]
80. Zhao, D.; Dong, C.; Wang, B.; Chen, C.; Huang, Y.; Diao, Z.; Li, S.; Guo, L.; Shen, S. Synergy of dopants and defects in graphitic carbon nitride with exceptionally modulated band structures for efficient photocatalytic oxygen evolution. *Adv. Mater.* **2019**, *31*, 1903545. [CrossRef]
81. Han, X.; Xu, D.; An, L.; Hou, C.; Li, Y.; Zhang, Q.; Wang, H. Ni-Mo nanoparticles as co-catalyst for drastically enhanced photocatalytic hydrogen production activity over g-C_3N_4. *Appl. Catal. B-Environ.* **2019**, *243*, 136–144. [CrossRef]
82. Wu, X.; Gao, D.; Yu, H.; Yu, J. High-yield lactic acid-mediated route for a g-C_3N_4 nanosheet photocatalyst with enhanced H_2-evolution performance. *Nanoscale* **2019**, *11*, 9608–9616. [CrossRef] [PubMed]

83. Zhang, G.; Li, G.; Heil, T.; Zafeiratos, S.; Lai, F.; Savateev, A.; Antonietti, M.; Wang, X. Tailoring the grain boundary chemistry of polymeric carbon nitride for enhanced solar hydrogen production and CO_2 reduction. *Angew. Chem. Int. Ed.* **2019**, *58*, 3433–3437. [CrossRef] [PubMed]
84. Khan, I.; Luo, M.; Khan, S.; Asghar, H.; Saeed, M.; Khan, S.; Khan, A.; Humayun, M.; Guo, L.; Shi, B. Green synthesis of SrO bridged $LaFeO_3$/g-C_3N_4 nanocomposites for CO_2 conversion and bisphenol A degradation with new insights into mechanism. *Environ. Res.* **2022**, *7*, 112650. [CrossRef] [PubMed]
85. Zhang, J.; Su, F.; Wen, P.; Wang, Y.; Zhao, B.; Jiang, L.; Sun, Y. In situ growth of Co_2P nanocrystal on g-C_3N_4 for efficient and stable photocatalytic hydrogen evolution. *Energy Fuels* **2021**, *35*, 1859–1865. [CrossRef]
86. Zhang, J.; Wu, M.; He, B.B.; Wang, R.; Wang, H.W.; Gong, Y.S. Facile synthesis of rod-like g-C_3N_4 by decorating Mo_2C co-catalyst for enhanced visible-light photocatalytic activity. *Appl. Surf. Sci.* **2019**, *470*, 565–572. [CrossRef]
87. Yuan, Y.J.; Shen, Z.; Wu, S.; Su, Y.; Pei, L.; Ji, Z.; Ding, M.; Bai, W.; Chen, Y.; Yu, Z.T.; et al. Liquid exfoliation of g-C_3N_4 nanosheets to construct 2D-2D MoS_2/g-C_3N_4 photocatalyst for enhanced photocatalytic H_2 production activity. *Appl. Catal. B-Environ.* **2019**, *246*, 120–128. [CrossRef]
88. Zhang, S.; Dong, H.; An, C.; Li, Z.; Xu, D.; Xu, K.; Wu, Z.; Shen, J.; Chen, X.; Zhang, S. One-pot synthesis of array-like sulfur-doped carbon nitride with covalently crosslinked ultrathin MoS_2 cocatalyst for drastically enhanced photocatalytic hydrogen evolution. *J. Mater. Sci. Technol.* **2021**, *75*, 59–67. [CrossRef]
89. Li, J.; Wu, W.; Li, Y.; Zhang, H.; Xu, X.; Jiang, Y.; Lin, K. In situ synthesized rodlike MoS_2 as a cocatalyst for enhanced photocatalytic hydrogen evolution by graphitic carbon nitride without a noble metal. *ACS Appl. Energy Mater.* **2021**, *4*, 11836–11843. [CrossRef]
90. Zhang, Y.; Wan, J.; Zhang, C.; Cao, X. MoS_2 and Fe_2O_3 co-modify g-C_3N_4 to improve the performance of photocatalytic hydrogen production. *Sci. Rep.* **2022**, *12*, 3261. [CrossRef]
91. Li, X.; Lv, X.; Li, N.; Wu, J.; Zheng, Y.Z.; Tao, X. One-step hydrothermal synthesis of high-percentage 1T-phase MoS_2 quantum dots for remarkably enhanced visible-light-driven photocatalytic H_2 evolution. *Appl. Catal. B-Environ.* **2019**, *243*, 76–85. [CrossRef]
92. Liang, Z.; Sun, B.; Xu, X.; Cui, H.; Tian, J. Metallic 1T-phase MoS_2 quantum dots/g-C_3N_4 heterojunctions for enhanced photocatalytic hydrogen evolution. *Nanoscale* **2019**, *11*, 12266–12274. [CrossRef] [PubMed]
93. Liang, Z.; Guo, Y.; Xue, Y.; Cui, H.; Tian, J. 1T-phase MoS_2 quantum dots as a superior co-catalyst to Pt decorated on carbon nitride nanorods for photocatalytic hydrogen evolution from water. *Mater. Chem. Front.* **2019**, *3*, 2032–2040. [CrossRef]
94. Shi, J.; Zou, Y.; Ma, D.; Fan, Z.; Cheng, L.; Sun, D.; Wang, Z.; Niu, C.; Wang, L. Stable 1T-phase MoS_2 as an effective electron mediator promoting photocatalytic hydrogen production. *Nanoscale* **2018**, *10*, 9292–9303. [CrossRef]
95. Yu, H.; Xiao, P.; Wang, P.; Yu, J. Amorphous molybdenum sulfide as highly efficient electron-cocatalyst for enhanced photocatalytic H_2 evolution. *Appl. Catal. B-Environ.* **2016**, *193*, 217–225. [CrossRef]
96. Peng, X.; Huang, C.; Zhang, B.; Liu, Y. Atomic-scale intercalation of amorphous MoS_2 nanoparticles into N-doped carbon as a highly efficient electrocatalyst for hydrogen evolution reaction. *Int. J. Hydrogen Energy* **2020**, *45*, 27193–27201. [CrossRef]
97. Lee, S.C.; Benck, J.D.; Tsai, C.; Park, J.; Koh, A.L.; Abild-Pedersen, F.; Jaramillo, T.F.; Sinclair, R. Chemical and phase evolution of amorphous molybdenum sulfide catalysts for electrochemical hydrogen production. *ACS Nano* **2016**, *10*, 624–632. [CrossRef]
98. Zhang, Z.W.; Li, Q.H.; Qiao, X.Q.; Hou, D.; Li, D.S. One-pot hydrothermal synthesis of willow branch-shaped MoS_2/CdS heterojunctions for photocatalytic H_2 production under visible light irradiation. *J. Catal.* **2019**, *40*, 371–379. [CrossRef]
99. Ma, S.; Xie, J.; Wen, J.Q.; He, K.L.; Li, X.; Liu, W.; Zhang, X.C. Constructing 2D layered hybrid CdS nanosheets/MoS_2 heterojunctions for enhanced visible-light photocatalytic H_2 generation. *Appl. Surf. Sci.* **2017**, *391*, 580–591. [CrossRef]
100. Patriarchea, C.; Vamvasakis, I.; Koutsouroubi, E.D.; Armatas, G.S. Enhancing interfacial charge transfer in mesoporous MoS_2/CdS nanojunction architectures for highly efficient visible-light photocatalytic water splitting. *Inorg. Chem. Front.* **2022**, *9*, 625–636. [CrossRef]
101. Samaniego-Beniteza, J.E.; Lartundo-Rojas, L.; García-Garcíac, A.; Calderón, H.A.; Mantilla, A. One-step synthesis and photocatalytic behavior for H_2 production from water of ZnS/MoS_2 composite material. *Catal. Today* **2021**, *360*, 99–105. [CrossRef]
102. Guan, W.; Li, Y.; Zhong, Q.; Liu, H.; Chen, J.; Hu, H.; Lv, K.; Gong, J.; Xu, Y.; Kang, Z.; et al. Fabricating $MAPbI_3$/MoS_2 Composites for improved photocatalytic performance. *Nano Lett.* **2021**, *21*, 597–604. [CrossRef] [PubMed]
103. Meng, A.Y.; Zhang, J.; Xu, D.F.; Cheng, B.; Yu, J.G. Enhanced photocatalytic H_2-production activity of anatase TiO_2 nanosheet by selectively depositing dual-cocatalysts on {101} and {001} facets. *Appl. Catal. B-Environ.* **2016**, *198*, 286–294. [CrossRef]
104. Meng, A.; Zhang, L.; Cheng, B.; Yu, J. Dual Cocatalysts in TiO_2 Photocatalysis. *Adv. Mater.* **2019**, *31*, 1807660. [CrossRef]
105. Zhao, S.; Xu, J.; Li, Z.T.; Liu, Z.Y.; Li, Y.R. Molybdenum disulfide coated nickel-cobalt sulfide with nickel phosphide loading to build hollow core-shell structure for highly efficient photocatalytic hydrogen evolution. *J. Colloid. Interf. Sci.* **2019**, *555*, 689–701. [CrossRef]
106. Li, X.; Yu, J.; Jaroniec, M.; Chen, X. Cocatalysts for selective photoreduction of CO_2 into solar fuels. *Chem. Rev.* **2019**, *119*, 3962–4179. [CrossRef]
107. Lee, G.J.; Hou, Y.H.; Chen, C.Y.; Tsay, C.Y.; Chang, Y.C.; Chen, J.H.; Horng, T.L.; Anandan, S.; Wu, J.J. Enhanced performance for photocatalytic hydrogen evolution using MoS_2/graphene hybrids. *Int. J. Hydrogen Energy* **2021**, *46*, 5938–5948. [CrossRef]
108. Wang, X.; Long, R. Rapid charge separation boosts solar hydrogen generation at the graphene–MoS_2 Junction: Time-domain Ab initio analysis. *J. Phys. Chem. Lett.* **2021**, *12*, 2763–2769. [CrossRef]
109. Lu, X.Y.; Xie, J.; Chen, X.B.; Li, X. Engineering MPx (M = Fe, Co or Ni) interface electron transfer channels for boosting photocatalytic H_2 evolution over g-C_3N_4/MoS_2 layered heterojunctions. *Appl. Catal. B-Environ.* **2019**, *252*, 250–259. [CrossRef]

110. Cao, D.; Wang, Q.; Zhu, S.; Zhang, X.; Li, Y.; Cui, Y.; Xue, Z.; Gao, S. Hydrothermal construction of flower-like MoS_2 on TiO_2 NTs for highly efficient environmental remediation and photocatalytic hydrogen evolution. *Sep. Purif. Technol.* **2021**, *265*, 118463. [CrossRef]
111. Jiao, Y.; Huang, Q.; Wang, J.; He, Z.; Li, Z. A novel MoS_2 quantum dots (QDs) decorated Z-scheme g-C_3N_4 nanosheet/N-doped carbon dots heterostructure photocatalyst for photocatalytic hydrogen evolution. *Appl. Catal. B-Environ.* **2019**, *247*, 124–132. [CrossRef]
112. Feng, C.; Chen, Z.; Hou, J.; Li, J.; Li, X.; Xu, L.; Sun, M.; Zeng, R. Effectively enhanced photocatalytic hydrogen production performance of one-pot synthesized MoS_2 clusters/CdS nanorod heterojunction material under visible light. *Chem. Eng. J.* **2018**, *345*, 404–413. [CrossRef]
113. Wei, L.; Chen, Y.; Lin, Y.; Wu, H.; Yuan, R.; Li, Z. MoS_2 as non-noble-metal co-catalyst for photocatalytic hydrogen evolution over hexagonal $ZnIn_2S_4$ under visible light irradiations. *Appl. Catal. B-Environ.* **2014**, *144*, 521–527. [CrossRef]
114. Chen, G.; Ding, N.; Li, F.; Fan, Y.; Luo, Y.; Li, D.; Meng, Q. Enhancement of photocatalytic H_2 evolution on $ZnIn_2S_4$ loaded with in-situ photo-deposited MoS_2 under visible light irradiation. *Appl. Catal. B-Environ.* **2019**, *241*, 130–140. [CrossRef]
115. Wang, J.; Luo, J.; Liu, D.; Chen, S.; Peng, T. One-pot solvothermal synthesis of MoS_2-modified $Mn_{0.2}Cd_{0.8}S$/MnS heterojunction photocatalysts for highly efficient visible-light-driven H_2 production. *Appl. Catal. B-Environ.* **2014**, *160–161*, 614–620. [CrossRef]